Journal of Alloys and Compounds 505 (2010) 416–422

Contents lists available at ScienceDirect

Journal of Alloys and Compounds

journal homepage: www.elsevier.com/locate/jallcom

Structural and optoelectronic properties of antimony incorporated tin oxide thin films

A.R. Babar[a], S.S. Shinde[a], A.V. Moholkar[b,c], C.H. Bhosale[a], J.H. Kim[c], K.Y. Rajpure[a,*]

[a] Electrochemical Materials Laboratory, Department of Physics, Shivaji University, Kolhapur 416 004, India
[b] Department of Physics, Gopal Krishna Gokhale College, Kolhapur 416 012, M.S., India
[c] Department of Materials Science and Engineering, Chonnam National University, 300 Yongbong-Dong, Buk-Gu, Gwangju, 500-757, South Korea

ARTICLE INFO

Article history:
Received 25 February 2010
Received in revised form 2 June 2010
Accepted 12 June 2010
Available online 25 June 2010

Keywords:
$Sb:SnO_2$ thin films
X-ray diffraction
FE-SEM
XPS
Optical
PL
Electrical properties

ABSTRACT

Thin films of undoped and antimony doped tin oxide (SnO_2 and $Sb:SnO_2$) prepared by spray pyrolysis technique with different antimony concentrations are found to be polycrystalline with tetragonal crystal structure, having preferential growth along the (2 1 1) and (1 1 2) planes. Randomly oriented needle-shaped polyhedron like grains are observed in the FE-SEM images owing to large scattering effect in the films. From X-ray photoelectron spectroscopy (XPS) measurement, it is observed that films are oxygen deficient. Concentration of Sb in the SnO_2 films is slightly less than that of starting solution. Valence states for Sn, Sb and O, observed from the XPS measurement are Sn^{4+}, Sb^{5+}/Sb^{3+} and O_2^{2-}, respectively. The direct optical band gap (E_g) has increased from 3.55 (undoped) to 3.60 eV with Sb concentration showing formation of degenerate semiconductor. The strong violet and comparatively weak red emissions have observed in room temperature photoluminescence (PL). The origin of various peaks in PL spectra can be assigned to the combined effect of oxygen vacancies, tin interstitials or dangling bonds, singly charged oxygen vacancies, interstitial oxygen and crystal defects present in the films. The films deposited with 2 at.% Sb exhibited lowest value of resistivity ($1.22 \times 10^{-3}\ \Omega$ cm) and highest value of carrier concentration ($5.19 \times 10^{20}\ cm^{-3}$), mobility ($9.83\ cm^2\ V^{-1}\ s^{-1}$) and figure of merit ($2.11 \times 10^{-3}\ \Omega^{-1}$).

1. Introduction

The significant focus of thin film technology has been the development of transparent and conducting oxide (TCO) coatings that serve as window layers in photovoltaic devices and also as electrical contacts [1]. Now-a-days TCO materials having high mobility and increased conductivity with good transparency are extensively studied [2]. Since, last two decades, tin doped indium oxide (ITO) and fluorine doped tin oxide (FTO) thin films are essentially preferred in the semiconductor industries in highly sophisticated fields of science and technology [3]. In spite of excellent optoelectronic properties, ITO and FTO suffer from the sophistication of instability under reducing plasma at elevated temperatures. Further, the deficiency in supply of rare, expensive, toxic indium and fluorine required for the production of ITO and FTO thin films might be the cause of disquiet to the environment. As a result, many attempts have been made to build the potential substitute to these well-recognized materials. The Sb doped tin oxide (ATO) thin films are considered as an alternative to ITO and FTO due to its excellent heat resistivity [4]. Many dopants, such as W [5], Al [6], In [7], F [8], Si [9], La [10], Ni [11], Pt [12], Vd [13], Pd [14], Fe [15] and Sb [16] have been used to improve the electrical properties of tin oxide thin films. But in case of Sb doping, antimony presents a real challenge to electronic structure calculation in order to explain its optoelectronic properties [17]. Tin oxide with high doping concentration of antimony exhibits quasimetallic conductivity while maintaining its transparency in the optical region [18]. These interesting optoelectronic properties are exploited in solar cells and optical devices. ATO thin films are deposited by various methods viz. sputtering [19], vacuum evaporation [20], chemical vapour deposition [21], DC glow discharge [22], sol–gel [16,23] and spray pyrolysis [24–27]. Spray Pyrolysis is a promising technique for producing sufficiently conductive $Sb:SnO_2$ thin films in a cost-effective way. Though numerous amount of literature is available on spray deposition of ATO thin films, the efforts are made either to achieve high values for figure of merit or to achieve higher gas sensitivity in sensor applications by tailoring its crystalline structure and surface morphology. In the present study, we have made a specific effort to achieve the combined effect of ATO films to work as multi task film. The effect of Sb doping on film structure and morphology, optical and electrical properties of the films has been reported.

* Corresponding author. Tel.: +91 231 2609435; fax: +91 231 2691533.
E-mail address: rajpure@yahoo.com (K.Y. Rajpure).

0925-8388/$ – see front matter © 2010 Elsevier B.V. All rights reserved.
doi:10.1016/j.jallcom.2010.06.091

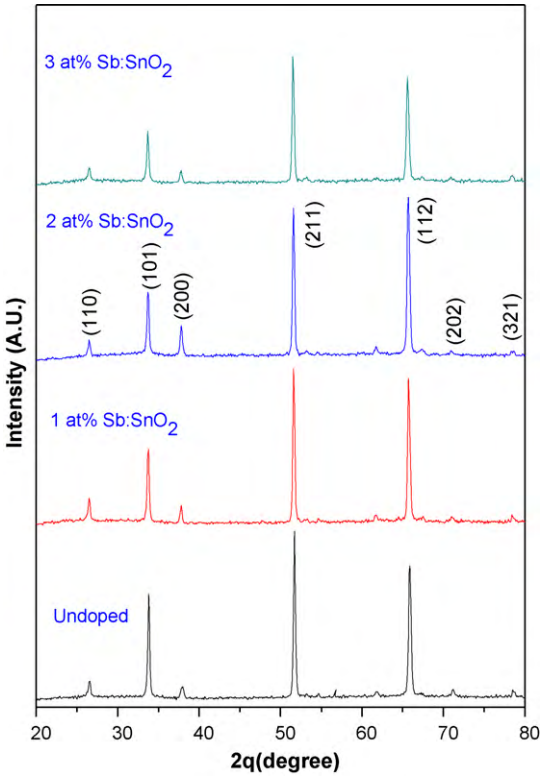

Fig. 1. X-ray diffraction patterns of undoped and Sb:SnO_2 thin films prepared with different Sb concentrations (in starting solution).

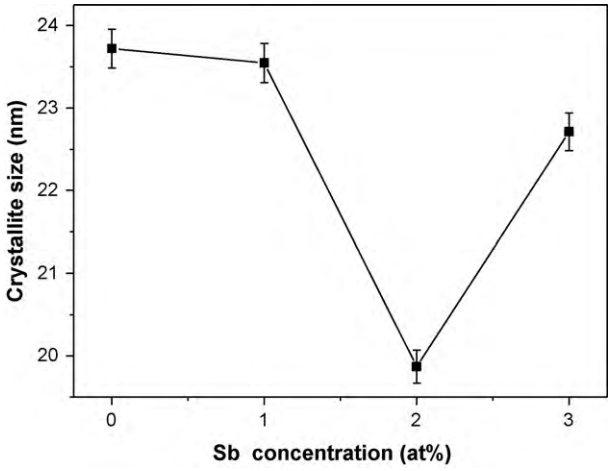

Fig. 2. Variation of the average crystallite size with different Sb concentrations.

2. Experimental

Undoped and Sb:SnO_2 thin films were deposited onto the ultrasonically cleaned preheated corning glass substrates using the chemical spray pyrolysis technique. Varying amounts of $SbCl_3$ dissolved in 1 M HCl was added to 2 M aqueous $SnCl_4{\cdot}5H_2O$ solution to obtain 1, 2 and 3 at.% Sb concentration in the starting solution. This was taken as the stock solution. Ten milliliters of propan-2-ol was added to the 10 ml of stock solution before spraying. The other deposition parameters such as spray rate (5 cc min^{-1}), nozzle to substrate distance (33 cm) were kept at their fixed values and ambient compressed air was used as a carrier gas. The resulting solution (20 ml) was sprayed at an optimized substrate temperature of 748 K.

The structural properties were studied by Powder X-ray diffractometer [Bruker D8 Advance, France] using Cu Kα radiation in the 2θ range of 20–80°. The morphology of the films was observed by using field emission scanning electron microscopy (FE-SEM, Model: JSM-6701F, Japan). XPS studies were carried out using the model PHI-5400 type X-ray photoelectron spectroscopy (XPS, Physical Electronics PHI 5400, USA) with monochromatic Mg Kα (1254 eV) radiation. Optical absorption study was carried out in the wavelength range 250–1100 nm using double beam spectrophotometer (SHIMADZU UV-1700, Japan). The room temperature photoluminescence (PL) spectra of the annealed samples were recorded using a PerkinElmer luminescence spectrometer (Model: LS55, USA). All spectra were measured at room temperature with an Ar ion laser as a light source using an excitation wavelength 325 nm. The electrical measurements like resistivity (ρ), sheet resistance (R_{sh}), carrier concentration (n) and mobility (μ) were carried out at room temperature by using Hall effect setup (Scientific Instruments, DHE-21, Roorkee, India) in Van der Pauw configuration.

3. Results and discussion

3.1. X-ray diffraction (XRD) studies

Fig. 1 show the XRD patterns of undoped and Sb:SnO_2 thin films deposited for different antimony concentrations. It is seen that the films exhibit polycrystalline nature with tetragonal crystal structure having a preferential growth along the (2 1 1) and (1 1 2) planes, the unique observation in the present study compared to previous reports [28,29]. However, relative intensities of all the peaks go on decreasing with Sb doping concentration except for (1 1 2). Peak intensity of (1 1 2) plane increases up to 2 at.% Sb and then decreases slightly for higher Sb doping concentration, indicating slight reorientation effect. The Sb atoms substitutes to the Sn atoms up to 2 at.% Sb doping while for higher Sb doping concentrations (>2 at.%), Sb atoms goes to substitutional as well as interstitial sites in the SnO_2 lattice. Other weak intensity peaks viz. (1 1 0), (1 0 1), (2 0 0), (2 0 2) and (3 2 1) are also observed.

The crystallite size 'D' is calculated using Scherrer's formula,

$$D = \frac{0.9\lambda}{(\beta \cos\theta)} \quad (1)$$

where D is the crystallite size, β is the broadening of the diffraction line measured at half of its maximum intensity (rad) FWHM and λ is the X-ray wavelength (1.5406 Å). From Fig. 2, it is seen that as Sb concentration increases, the average crystallite size decreases up to 2 at.% and tends to increase afterwards. This effect can be explained, if it is considered that antimony atoms do not substitute tin atoms; instead they occupy interstitial sites resulting in a large number of dislocations.

The reflection intensities from each XRD pattern contain information related to the preferential or random growth of polycrystalline thin films which is studied by calculating the texture coefficient TC($h\,k\,l$) for the planes using the equation,

$$TC_{(h\ k\ l)} = \frac{I_{(h\,k\,l)}/I_0}{(1/N)\sum I_{(h\,k\,l)}/I_0} \quad (2)$$

where $I_{(h\,k\,l)}$ is the measured intensity of X-ray reflection, $I_{0(h\,k\,l)}$ is the corresponding standard intensity from the [JCPDS data card No-01-0625] and N is the number of reflections observed in the XRD pattern. Fig. 3 depicts the variation of the texture coefficient with Sb concentration for the (1 0 1), (2 1 1) and (1 1 2) planes. TC (1 1 2) for all the films has a relatively higher value than the other planes (1 0 1) and (2 1 1). TC of (1 1 2) plane slightly increases up to 2 at.% [Sb] doping and decreases with further increase in doping, while TC of (1 0 1) and (2 1 1) planes show a reverse trend. This confirms the reorientation effect with Sb concentration observed in ATO thin films.

3.2. Surface morphological study

Fig. 4(a–d) shows the FE-SEM images of the undoped and Sb:SnO_2 thin films. The films deposited by spray are found to be uniform. The surface morphology of the films is strongly dependent upon the Sb concentration. Here, we observed the two types of grains, which they named 'bigger' and twisted metal sheet like shape of grains and smaller and needle-shaped grains. Smaller and

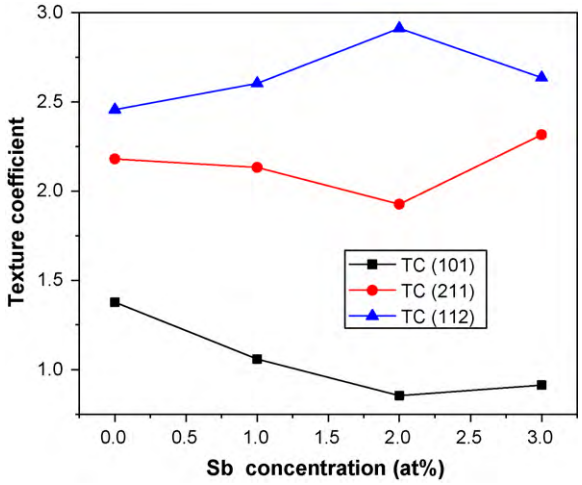

Fig. 3. Variation of TC (1 0 1), TC (2 1 1) and TC (1 1 2) with Sb concentration for Sb:SnO_2 thin films.

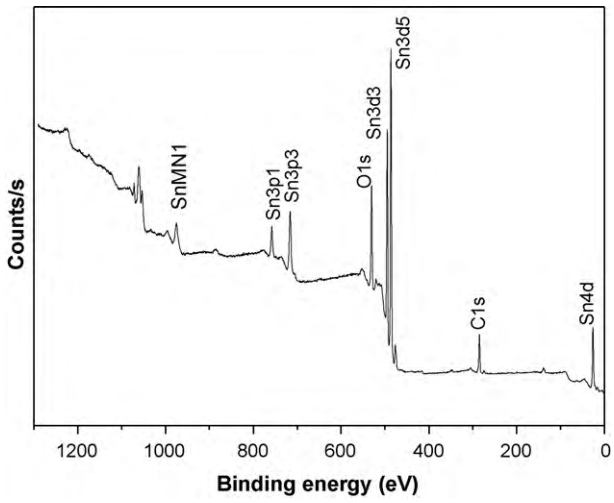

Fig. 5. XPS spectra of the typical 2 at.% Sb:SnO_2 thin film.

needle-shaped polyhedrons like grains are appeared on the surface of the pure tin oxide thin films. The grain sizes measured with FE-SEM images are 300–500 Å (large polyhedron like grains) and 100–200 Å (small grains). The number of needle-shaped grains decreases with increase in Sb doping levels. As the Sb concentration increases the polyhedron like grains dwindled and converted into twisted large round grains [30,31]. The grains are randomly grown giving rise to scattering effect thereby reducing transmittance.

3.3. XPS analysis

Fig. 5 shows the typical X-ray photoelectron spectroscopy (XPS) analysis scan of Sb:SnO_2 thin film deposited with 2 at.% Sb concentration. Sample contains the Sn, Sb, O and traces of C having Sn MN1 auger peak due to X-ray induced Auger emission with Sn 3p, Sn 3d, Sn 4d core levels. The presence of C 1s at 285 eV is attributed to contamination which resulted from the samples being exposed to air before the XPS measurements [32]. The binding energy of Sn $3d_{5/2}$ for all samples shows the Sn^{4+} bonding state from SnO_2. The narrow scan spectra for tin, antimony and oxygen are shown in Fig. 6(a–c). The spectrum reveals the spin-orbit splitting of the Sn $3d_{5/2}$ ground state and Sn $3d_{3/2}$ excited state core levels of tin in 486–487 and 494.88–495.39 eV, respectively with a better symmetry assigned to the lattice tin, Fig. 6(a). The separation between the Sn $3d_{5/2}$ and Sn $3d_{3/2}$ levels (8.5 eV) is approximately same with earlier reported spectrum of Sn [33]. Chemical shift observed for doublet $Sn3d_{5/2}$ and $Sn3d_{3/2}$ core states with respect to Sb doping concentration are in the range of 1.55–1.9 and 0.95–1.3 eV, respectively due to change in oxidation state of the atom and local chemical and physical environment. Atoms of a higher positive oxidation state exhibit a higher

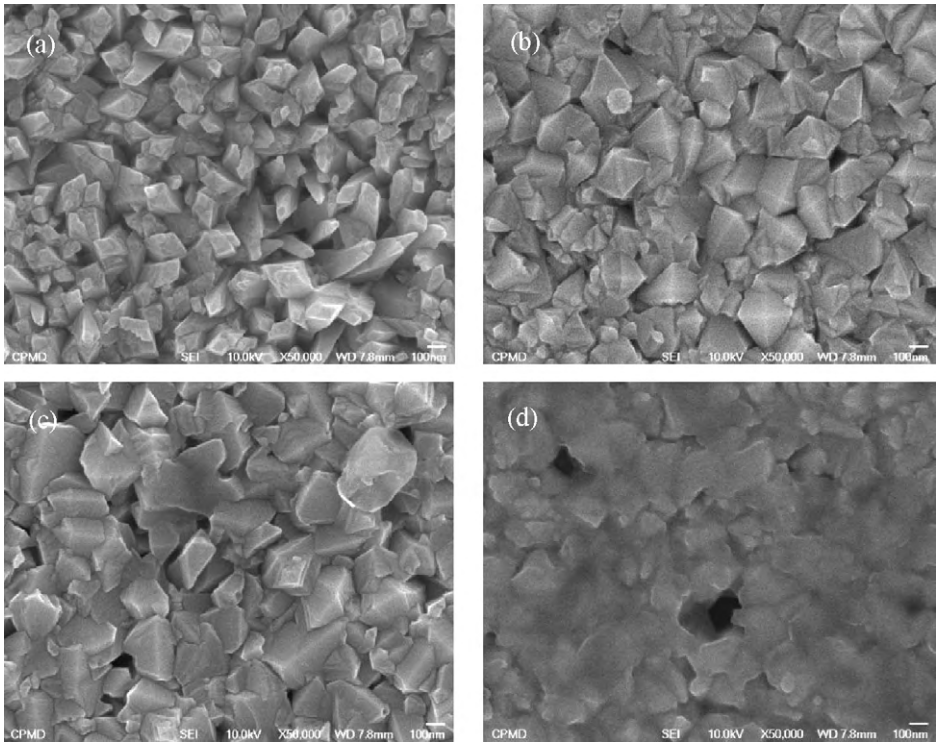

Fig. 4. SEM micrographs of (a) undoped, (b) 1 at.% (c) 2 at.% and (d) 3 at.% Sb:SnO_2 thin films.

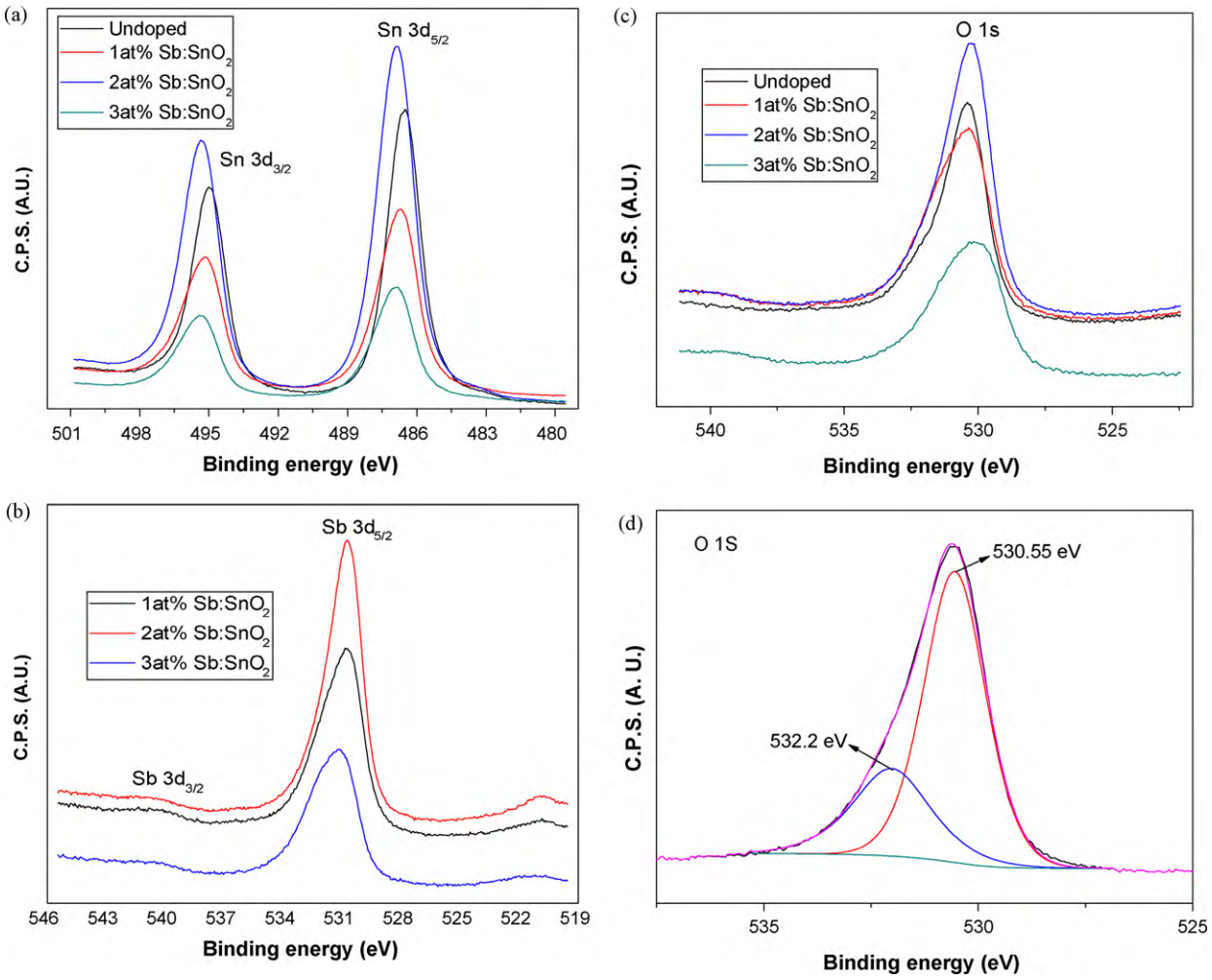

Fig. 6. XPS spectra of the Sb:SnO_2 thin films with Sb concentration (a) narrow scans of Sn 3d; (b) Sb 3d; (c) O 1s; (d) Gaussian fitted narrow scan of O 1s.

binding energy due to the extra coulombic interaction between the photo-emitted electron and the ion core.

The peaks of $Sb3d_{5/2}$ and $Sb3d_{3/2}$ are observed at 530.80, 530.72 and 531.21 and 540.30, 540.63 and 540.46 eV corresponding to 1–3 at.% Sb doping concentration, respectively, shown in Fig. 6(b). The shift in $Sb3d_{5/2}$ and $Sb3d_{3/2}$ is about 2.72–3.21 and 3.3–3.63 eV, respectively, indicating the presence of oxygen (O) bonding with Sn^{4+} and Sb^{5+}. Calculation of relative peak area confirms the dominance of Sb^{5+} ions over Sb^{3+} ions showing improvement in the conductivity by donating one extra electron. This behavior is further recognized through the electrical conductivity measurements.

The oxygen peaks for the undoped, 1 at.% Sb, 2 at.% Sb and 3 at.% Sb doped samples are observed at 530.67, 530.56, 530.93, 531.46 eV respectively (Fig. 6(c)). This can be attributed to O^{2-} state at lattice oxygen in non-stoichiometric oxides showing close agreement with reported values [32]. Gaussian curve fitting of typical 2 at.% Sb sample, (Fig. 6(d)) illustrates the O 1s peak has doublet component; such phenomenon is common for oxides containing oxygen in multiple valence states [34]. The 532.2 eV peak on the higher binding energy side of the O 1s spectrum can be attributed to O_2^{2-} state elemental oxygen (Oxygen sufficient states). The oxygen deficient states (62–72%) increases from undoped to 2 at.% Sb doping concentration and then decreases which is consistent with observed electrical conductivity and luminescence states. It can be seen that the oxygen peak in the spectra is asymmetric, which is due to the concealed Sb 3d peak. The chemical shift for higher doping is due to variation in concentration of the oxygen vacancies (ratio of sufficient to deficient states) [35]. The oxygen deficiency drastically alters the electronic properties, making the hopping of electrons between oxygen vacancies. This oxygen deficiency may also be useful for gas sensing property.

3.4. Optical properties

Fig. 7 shows the optical transmittance curves as a function of wavelength of the undoped and Sb:SnO_2 thin films. It is observed that, the transmittance increases with the increase in doping up to 2 at.% and decreases for further doping. Higher antimony doping imparted blue coloration to the films which further reduces the transmittance. The average transparency in the visible range is around ~80%. The decrease in transmittance at higher doping concentration may be due to the enhancement in photon scattering because of crystal defects created by antimony doping. Transmittance of TCO thin films prepared by spray technique is generally limited by: (i) reflection losses including specular and scattered (diffuse) components due to surface roughness and (ii) inhomogeneities in the film in terms of unreacted chemical species generated during the complex pyrolytic process [17]. However, the transmittance curves are distinguished by their gradients owing to the Sb concentration. In case of heavily doped semiconductors having carrier concentration 10^{19}–10^{21} cm^{-3}, the Drude's model is generally used for the attribution of the decrease in the transmittance [36]. Briefly, this model illustrates the drop in transmittance in the near infrared region is associated with the plasma frequency

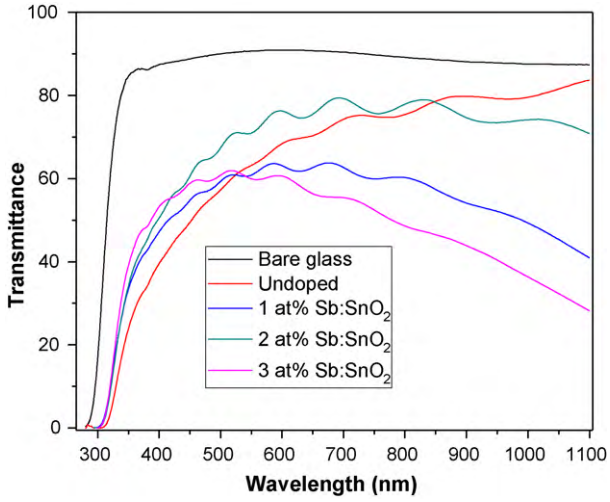

Fig. 7. The optical transmittance spectra of undoped and Sb:SnO_2 thin films prepared for different Sb concentrations (in starting solution).

(ω_p) expressed as,

$$\omega_p = \left(\frac{4\pi ne^2}{\varepsilon_0 \varepsilon_\infty m_c*}\right)^{1/2} \quad (3)$$

where n is the carrier concentration, e the electronic charge, ε_0 the permittivity of free space, ε_∞ the high-frequency permittivity and m_c^* the effective mass. As ω_p is proportional to the square root of carrier concentration, increase in carrier concentration leads to the lowering of transmission level in near IR region. The direct optical band gap (E_g) has increased from 3.55 to 3.60 eV with Sb concentration which is attributed to Moss–Burstein effect. This effect occurs owing to filling up of low energy levels by conduction electrons. Since, the Fermi level lies within the conduction band where its position depends on the density of free electrons, band gap energy determined in this way is not an actual band gap of the deposit as these are degenerate semiconductors. Thus, the optical band gaps are related to the excitation of the electrons from the valance band to the Fermi level in the conduction band, whereas the actual band gap of the material is related to the excitation of the electrons from the top of the valence band to the bottom of the conduction band. This means that there is lifting of the Fermi level into the conduction band of the degenerate semiconductor due to the increase in the carrier density leads to the energy band broadening (shifting).

3.5. Photoluminescence studies

The room temperature PL emission spectra of the undoped and Sb:SnO_2 thin films recorded in the range 350–850 nm is shown in Fig. 8(a). For undoped and doped samples, an intensive violet emission peak at 395 nm (about 3.14 eV) and shoulders at 366, 424 and 474 nm (3.39, 2.92 and 2.62 eV) are observed. In addition to this, there is a broad peak at 661 and 718 nm (about 1.88 and 1.73 eV). The inset shows the PL intensity brightness (violet peak) against antimony concentration. With increase in Sb concentration, the intensity of violet peak increases and attains maximum value at 2 at.% Sb concentration due to decrease in number of defects and the non-radiative recombination [37]. The high density of oxygen vacancies interact with interfacial tin leads to the formation of a considerable amount of trapped states within the band gap giving rise to high PL intensity at room temperature. Fig. 8(b) depicts the Gaussian profile fitting of the typical sample prepared using 2 at.% Sb. The origin of peak at 395 nm (3.14 eV) is attributed to the electron transition from donor level formed by oxygen vacancies (V_O) or

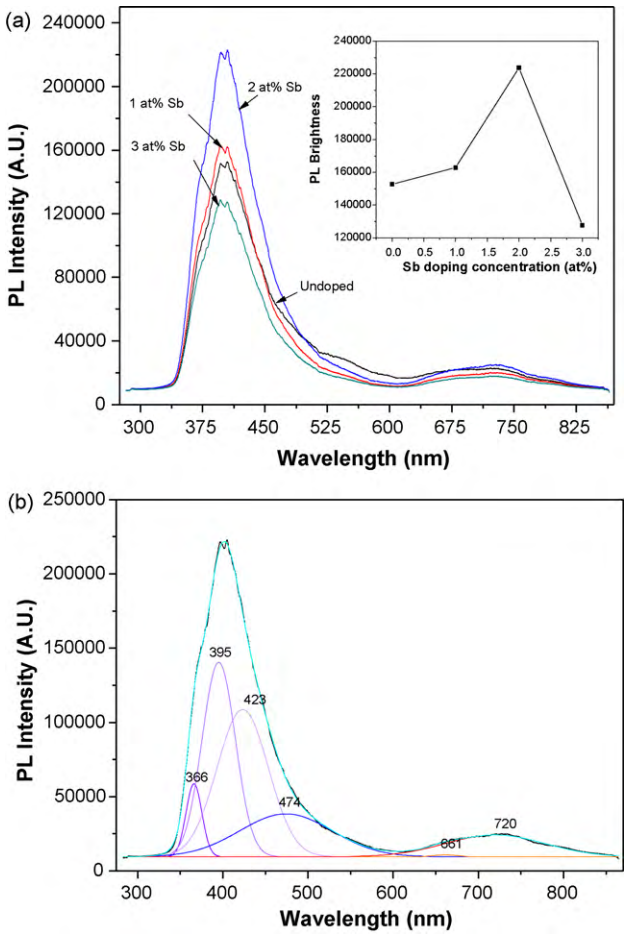

Fig. 8. (a) PL emission spectra of Sb:SnO_2 thin films with different Sb concentrations (the inset shows the plots of PL intensity versus Sb doping concentration); (b) Gaussian fitted typical PL spectrum of 2 at.% Sb:SnO_2.

Sb^{5+} ions to the acceptor level formed by Sb^{3+} ions [38]. The basis of peak at 424 nm can be ascribed to the luminescence centers formed by tin interstitials (Sn_i) or dangling bonds present in the SnO_2 thin films [39]. Other peak appeared at 474 nm, which corresponds to blue luminescence and can be attributed to singly charged oxygen vacancies (V_O) in the films. [40]. The orange emission observed at 661 nm might be due to involvement of an interstitial oxygen (O_i) ions [41]. Broad peak observed at 718 nm for all films may be due to other crystal defects which are formed during the growth of samples. Table 1 indicates the various emissions observed in undoped and Sb:SnO_2 thin films. It is seen that, there is slight shifting in emission lines due to dopant incorporation. Sn_i, O_i and V_O dominate in the defect structure of SnO_2 due to the multivalence of tin, explaining the natural non-stoichiometry of this material [42].

Table 1
Various PL emissions observed in undoped and Sb:SnO_2 thin films.

Sample	Peak position					
	V_1	V_2	V_3	B	O	R
Undoped	366	395	424	488	679	719
1% Sb	366	393	421	470	661	719
2% Sb	366	395	424	474	661	718
3% Sb	365	391	418	465	660	717

where V_1, V_2, V_3 correspond to Violet emission; B is Blue emission; O is Orange emission and R is Red emission.

Table 2
Various parameters estimated for sprayed Sb:SnO_2 thin films with different Sb concentrations.

Sb (at.%)	R_{sh} (Ω)	ρ (10^{-3} Ω cm)	n (10^{20} cm^{-3})	μ (cm^2 V^{-1} s^{-1})	ϕ (10^{-3} Ω^{-1})	E_f (eV)	l (Å)	t (nm)	C.S. (nm)	ω_p (10^{15} Hz)
0	77.95	6.33	2.59	3.81	0.13	0.78	4.9	812	23.72	2.33
1	31.31	2.51	3.81	6.53	0.23	1.0	9.6	802	23.54	2.83
2	15.42	1.22	5.19	9.83	2.11	1.24	16.0	794	19.87	3.31
3	30.75	2.45	4.60	5.54	0.20	1.14	8.6	797	22.71	3.11

3.6. Electrical properties

Analysis of the electrical properties of undoped and Sb:SnO_2 thin films is premeditated using Van der Pauw technique. The values of electrical resistivity along with other parameters with Sb concentration are tabulated in Table 2. As Sb concentration goes on increasing the resistivity decreases up to 2 at.% [Sb] and becomes minimum of 1.22×10^{-3} Ω cm and there after it slightly increases for higher concentrations. This is due to the fact that when antimony exceeds the limit of maximum solubility in tin oxide, it produces a grain boundary segregation of impurities which causes a dispersion of carriers. The Hall effect measurement confirms that the Sb:SnO_2 films exhibits the n-type conductivity.

Table 2 also depicts the carrier concentration (n) and carrier mobility (μ) of the Sb:SnO_2 thin film for different Sb concentrations. The carrier concentration of undoped film is 2.59×10^{20} cm^{-3} and there is an increase in carrier concentration up to 2 at.% Sb concentration. The maximum carrier concentration of 5.19×10^{20} cm^{-3} is observed for the films deposited with optimum Sb concentration of 2 at.%. With increase in Sb concentration the Hall mobility increases from 3.81 to 9.83 cm^2 V^{-1} s^{-1} and then decreases for heavy doping. The Hall mobility in doped semiconductors is usually limited by two major scattering mechanisms: grain boundary scattering and ionized impurity scattering [43].

The mean free path (l) is calculated by the following relation,

$$l = \frac{h}{2e}\left(\frac{3n}{\pi}\right)^{1/3}\mu \quad (4)$$

where h the Plank's constant, e the electron charge, n the carrier concentration and μ the Hall mobility. The mean free path increases with concentration up to 2 at.% (Table 2) and then decreases for higher concentrations. The films deposited at 2 at.% Sb concentration shows mean free path (l) is 16 Å. Since the l values are considerably shorter than the grain size (as seen in FE-SEM images) the Hall mobility is limited by the ionized impurity scattering rather than the grain boundary scattering.

The film degeneracy is confirmed by evaluating Fermi energy using relation,

$$\Delta E = \left(\frac{h^2}{8m*}\right)\left(\frac{3n}{\pi}\right)^{2/3} \quad (5)$$

The value of effective mass evaluated from plasma frequency for antimony doped SnO_2 films; $0.19m_e$ (m_e = rest mass of electron) is used in evaluating Fermi energy. The calculated value of Fermi energy lies in the range of 0.78–1.24 eV (Table 2). Fermi energy values are higher compared to kT at room temperature which is the evidence for degenerate nature of materials.

For optoelectronic device applications, the figure of merit (ϕ) plays an important role. The device performance is determined from ϕ and is calculated by using the Hacke's formula [44],

$$\phi = \frac{T^{10}}{R_{sh}} \quad (6)$$

where T the transmittance at 550 nm and R_{sh} the sheet resistance.

The sheet resistance (R_{sh}) is a main factor for figure of merit, which is calculated by van der Pauw technique. The variation of figure of merit with Sb concentration is shown in Fig. 9. As the Sb concentration increases, the figure of merit first increases and then decreases. The highest figure of merit obtained is 2.11×10^{-3} Ω^{-1} for 2 at.% Sb:SnO_2 films. This may be due to the fact that up to 2 at.% Sb concentration Sb^{5+} atoms replace the tin atoms in the SnO_2 lattice releasing one extra electron responsible for conduction. Observed figure of merit is relatively lower than reported by other groups, because the ATO films in the present study have low transmittance.

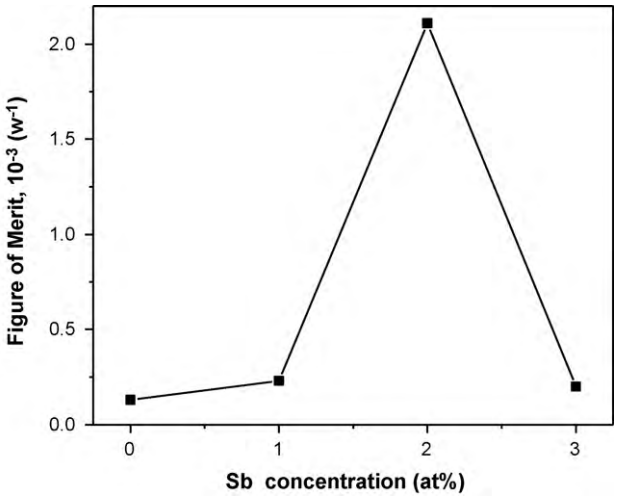

Fig. 9. Variation of figure of merit of Sb:SnO_2 thin films with different Sb concentration (in starting solution).

4. Conclusions

Undoped and Sb:SnO_2 thin films are successfully prepared using inexpensive spray pyrolysis technique. The films are polycrystalline with tetragonal crystal structure showing crystal reorientation effect as well as grain boundary scattering confirmed from SEM. Valence states for Sn, Sb and O, observed from the XPS measurement are Sn^{4+}, Sb^{5+}/Sb^{3+} and O_2^{2-}, respectively. Also it shows the symmetric spin-orbit splitting of Sn $3d_{5/2}$ ground state and Sn $3d_{3/2}$ excited states. The direct optical band gap (E_g) has increased from 3.55 (undoped) to 3.60 eV with Sb concentration showing formation of degenerate semiconductor. The dominant luminescent centers of strong violet emission have been confirmed from photoluminescence spectra. The highest figure of merit and the minimum resistivity achieved for Sb:SnO_2 thin films has been found to be 2.11×10^{-3} Ω^{-1} and 1.22×10^{-3} Ω cm, respectively. Enhancement in optoelectronic properties is due to oxygen deficiency have confirmed from the XPS analysis. The physico-chemical properties of these thin films indicate their possible candidature for application as multitask thin film devices (TCOs, optoelectronic devices and sensors) based on the antimony variation.

Acknowledgement

One of the authors (A.R. Babar) is highly grateful to University Grants Commission, New Delhi for its support through UGC meritorious fellowship.

References

[1] B.G. Lewis, D.C. Paine, MRS Bull. 25 (2000) 22.
[2] S. Jin, Y. Yang, J.E. Medvedeva, L. Wang, S. Li, N. Cortes, J.R. Ireland, A.W. Metz, J. Ni, M.C. Hersam, J. Freeman, T.J. Marks, Chem. Mater. 20 (2008) 220.
[3] M.M.B. Mohagheghi, M.S. Saremi, Semicond. Sci. Technol. 18 (2003) 97.
[4] S.Y. Lee, B.O. Park, Thin Solid Films 510 (2006) 154.
[5] Y. Huang, Q. Zhang, G. Li, M. Yang, Mater. Charact. 60 (2009) 415.
[6] J.S. Bhat, K.I. Maddani, A.M. Karguppikar, S. Ganesh, Nucl. Instrum. Methods Phys. Res. Sect. B: Beam Interact. Mater. Atoms 258 (2007) 369.
[7] Z.B. Zhou, R.Q. Cui, Q.J. Pang, Y.D. Wang, F.Y. Meng, T.T. Sun, Z.M. Ding, X.B. Yu, Appl. Surf. Sci. 172 (2001) 245.
[8] A.V. Moholkar, S.M. Pawar, K.Y. Rajpure, C.H. Bhosale, J.H. Kim, Appl. Surf. Sci. 255 (2009) 9358.
[9] H. Huang, E.M. Kelder, L. Chen, J. Schoonman, Solid State Ionics 120 (1999) 205.
[10] A. Marsal, A. Cornet, J.R. Morante, Sens. Actuators B: Chem. 94 (2003) 324.
[11] M.N. Rumyantseva, A.M. Gaskov, L.I. Ryabova, J.P. Senateur, B. Chenevier, M. Labeau, Mater. Sci. Eng. B 41 (1996) 333.
[12] M. Gaidi, B. Chenevier, M. Labeau, J.L. Hazemann, Sens. Actuators B: Chem. 120 (2006) 313.
[13] Chien-Tsung Wang, Miao-Ting Chen, Mater. Lett. 63 (2009) 389.
[14] Yisi Feng, Rishneg Yao, Lide Zhang, Mater. Chem. Phys. 89 (2005) 312.
[15] S. Chakraborty, A. Sen, H.S. Maiti, Sens. Actuators B: Chem. 115 (2006) 610.
[16] D. Zhang, L. Tao, Z. Deng, J. Zhang, L. Chen, Mater. Chem. Phys. 100 (2006) 275.
[17] K.L. Chopra, S. Major, D.K. Pandya, Thin Solid Films 102 (1983) 1–46.
[18] K.C. Mishra, K.H. Johnson, P.C. Schmidt, Phys. Rev. B. 51 (1995) 13972.
[19] D.B. Fraser, H.D. Cook, J. Electrochem. Soc. 119 (1972) 368.
[20] M. Mizuhashi, J. Non-Cryst. Solids 38 (1980) 329.
[21] J. Kane, H.P. Schweizer, W. Kern, J. Electrochem. Soc. 123 (1976) 270.
[22] D.E. Carlson, J. Electrochem. Soc. 122 (1975) 1334.
[23] D. Zhang, Z. Deng, J. Zhang, L. Chen, Mater. Chem. Phys. 98 (2006) 353.
[24] D. Zaouk, Y. Zaatar, A. Khoury, C. Llinares, J.P. Charles, J. Bechara, Microelectron. Eng. 51–52 (2000) 627.
[25] K.Y. Rajpure, M.N. Kusumade, N. Michael, C.H. Neumann-Spallart, Bhosale, Mater. Chem. Phys. 64 (2000) 184.
[26] S.M. Rozati, Mater. Charact. 57 (2006) 150.
[27] K. Ravichandran, G. Muruganantham, B. Sakthivel, Physica B 404 (2009) 4299.
[28] J. Ni, X. Zhao, X. Zheng, J. Zhao, B. Liu, Acta Mater. 57 (2009) 278.
[29] K. Ravichandran, P. Philominathan, Mater. Lett. 62 (2008) 2980.
[30] N.S. Baik, G. Sakai, K. Shimanoe, N. Miura, N. Yamazoe, Sens. Actuators B 65 (2000) 97.
[31] M. Losurdo, D. Barreca, P. Capezutto, G. Bruno, E. Tondello, Surf. Coat. Technol. 2 (2000) 151.
[32] D. Kim, S. Kim, Surf. Coat. Technol. 176 (2003) 23.
[33] H.-L. Ma, X.-T. Hao, J. Ma, Y.-G. Yang, J. Huang, D.-H. Zhang, X.-G. Xu, Appl. Surf. Sci. 191 (2002) 313.
[34] J.P. Bonnelle, J. Grimblot, A. D'huysser, J. Electron. Spectrosc. Relat. Phenom. 7 (1975) 151.
[35] T. Szörenyi, L.D. Laude, I. Bertoti, Z. Kantor, Z. Geretovszky, J. Appl Phys. 78 (1995) 6211.
[36] C. Marcel, N. Naghavi, G. Couturier, J. Salardenne, J.M. Tarascon, J. Appl. Phys. 91 (2002) 4291.
[37] Y. Wang, J. Ma, F. Ji, X. Yu, H. Ma, J. Lumin. 114 (2005) 71.
[38] T.W. Kim, D.U. Lee, Y.S. Yoon, J. Appl. Phys. 88 (2000) 3759.
[39] D. Calestani, L. Lazzarini, G. Salviati, M. Zha, Cryst. Res. Technol. 40 (2005) 937.
[40] S. Rani, S.C. Roy, N. Karar, M.C. Bhatnagar, Solid State Commun. 141 (2007) 214.
[41] D. Zhang, D. Guo, X. Pu, X. Shao, R. Liu, L. Li, X. Qian, Mater. Lett. 63 (2009) 2290.
[42] Çetin Kılıç, Alex Zunger, Phys. Rev. Lett. 88 (2002) 095501.
[43] B. Thangaraju, Thin Solid Films 402 (2002) 71.
[44] G. Haacke, J. Appl. Phys. 47 (1976) 4086.